Ultrafast Processing of Hierarchical Nanotexture for a Transparent Superamphiphobic Coating with Extremely Low Roll-Off Angle and High Impalement Pressure

Teisala, H., Geyer, F., Haapanen, J., Juuti, P., Mäkelä, J. M., Vollmer, D., et Butt, H.-J.

WILEY-VCH

DOI: 10.1002/((please add manuscript number))
Article type: Communication

Ultra-fast processing of hierarchical nanotexture for a transparent superamphiphobic coating with extremely low roll-off angle and high impalement pressure

Hannu Teisala[*], *Florian Geyer*, *Janne Haapanen*, *Paxton Juuti*, *Jyrki M. Mäkelä*, *Doris Vollmer*, *Hans-Jürgen Butt*[*]

Dr. H. Teisala, F. Geyer, Prof. D. Vollmer, Prof. H.-J. Butt
Max Planck Institute for Polymer Research, Department of Physics at Interfaces, Ackermannweg 10, D-55128 Mainz, Germany
E-mail: teisala@mpip-mainz.mpg.de and butt@mpip-mainz.mpg.de

J. Haapanen, P. Juuti, Prof. J.M. Mäkelä
Tampere University of Technology, Laboratory of Physics, P.O. Box 692, FI-33101 Tampere, Finland

Keywords: wetting, superhydrophobic, superoleophobic, omniphobic, spray coating

Low roll-off angle, high impalement pressure, and mechanical robustness are key requirements for super liquid-repellent surfaces to realize their potential in applications ranging from gas exchange membranes to protective and self-cleaning materials. Achieving these properties is still a challenge with superamphiphobic surfaces, which can repel both water and low-surface-tension liquids. In addition, fabrication procedures of superamphiphobic surfaces are typically slow and expensive. Here, by making use of liquid flame spray, we fabricate a silicon dioxide – titanium dioxide nanostructured coating at a high velocity up to 0.8 m/s. After fluorosilanization, the coating is superamphiphobic with excellent transparency and an extremely low roll-off angle; 10 µL drops of *n*-hexadecane roll off the surface at inclination angles even below 1°. Notably, the drops bounce off when impacting from a height of 50 cm, demonstrating the high impalement pressure of the coating. The extraordinary properties are due to a pronounced hierarchical nanotexture of the coating.

Superamphiphobic surfaces are characterized by their low adhesion to both polar and non-polar, low-surface-tension liquids.[1-5] Drops deposited on such surfaces adapt a spherical shape with an apparent receding contact angle[6] larger than ~140°. As a result, drops can roll off the surface at low inclination angles, typically below 10°. The first approaches to design superamphiphobic surfaces were introduced by Tsujii et al.[1] in 1997 and Tuteja et al.[2] in 2007. After this, superamphiphobic surfaces have been in spotlight of research both from the fundamental and economical aspects. Full comprehension of the super liquid-repellency mechanisms is a prerequisite to realize the potential of superamphiphobic surfaces in applications ranging from protective and self-cleaning materials[4, 7] to medical devices[8, 9] and gas exchange membranes.[10] In many of the applications, such as wind screens, window panes, lenses, or protective goggles, the superamphiphobic coating should be optically transparent, mechanically stable, and capable of repelling liquid impalement even under high hydrostatic pressure or drop impact.[11]

The capability of superamphiphobic surfaces to repel low-surface-tension liquids arises from a combination of their overhang, inward curved surface morphology and low-surface-energy chemistry. Overhanging morphology and low surface energy are required to stabilize an air cushion below the drops and maintain the so-called Cassie-Baxter state[12]. An exception to this is a doubly re-entrant micropillar surface introduced by Liu and Kim,[13] where a low-surface-energy chemistry is not needed. The required surface morphology for superamphiphobic materials can be realized with well-defined, mushroom-like micropillars[2, 13, 14] or with random, sub-micron scale surface textures with overhang curvature. The micropillars are typically fabricated by reactive ion etching.[2, 13] Randomly structured superamphiphobic surfaces have a higher potential for scaled up production. Methods to fabricate these surfaces include growth of silicone nanofilaments[3, 10] and templating candle soot.[4] Because the morphology required for superamphiphobic surfaces is rather complex,

the number of suitable approaches is limited. Most methods are energy-, chemical-, or time-consuming with multiple process steps.[5, 7] Furthermore, it is still a challenge to fabricate superamphiphobic surfaces which combine high receding contact angles with high impalement pressure and mechanical robustness.

Spray methods are potential candidates for scaled up fabrication of super liquid-repellent surfaces.[15, 16] Particularly, liquid flame spray (LFS) has been applied to produce superhydrophobic surfaces in high-speed roll-to-roll processes.[17-19] In LFS a liquid feedstock is injected and atomized in an oxygen-hydrogen flame. Dissolved in the liquid are organometallic precursor molecules. After evaporating and reacting in the flame they form nanoparticles. These nanoparticles are collected on the surface. With the heat from the flame the particles partially sinter together to form a stable, highly porous film. Advantages of LFS are that the deposition process is solvent-free and takes only fractions of seconds as the sample is rapidly moved through the flame spray even at the velocities of the order of m/s. In addition, a broad range of materials including vulnerable bio-materials such as cellulose-based paper and wood can be coated.[16, 20] A certain minimal velocity is required to avoid destroying the substrate.

Here we use LFS to fabricate a superamphiphobic and optically transparent silicon dioxide (SiO_2) – titanium dioxide (TiO_2) nanoparticle coating on glass. Our coating shows minimal solid–liquid interactions for both high- and low-surface-tension, polar and non-polar liquids. Drops of water and *n*-hexadecane (10 µL) deposited on the surface easily roll off the coating at inclination angles <1°. To our knowledge this is the lowest roll-off angle towards hexadecane ever reported. To achieve these superior properties, firstly, we adjusted the surface morphology by varying the ratio of silicon dioxide and titanium dioxide in the coating. Secondly, after achieving the right morphology, we applied chemical vapor

deposition (CVD) of a 1*H*,1*H*,2*H*,2*H*-perfluorooctyl-trichlorosilane (97% pure, Sigma-Aldrich) to lower the surface energy. In this way, we left the nanoporous morphology of the coating intact. This is necessary to achieve the superamphiphobic properties – already a 20-nm-thick additional layer on top of the nanoparticles hinders liquid repellency.

To synthesize the surfaces by LFS, we use hydrogen (50 L/min) and oxygen (15 L/min) as combustion gases to achieve a turbulent, high temperature flame (>2,500°C)[19] and inject the liquid feedstock, tetraethyl orthosilicate (TEOS, 98% pure, Alfa Aesar) and titanium(IV) isopropoxide (TTIP, 97% pure, Alfa Aesar) dissolved in isopropanol (technical grade, Neste), into the flame through a custom-made spray torch at a feed rate of 12 mL/min (the overall Si+Ti atomic concentration in the precursor solution was kept constant at 50 mg/mL), **Figure 1**. The organometallic precursors react and nucleate in the flame to form nanosized oxide particles. The particles aggregate and are deposited directly on the surface – driven by diffusion and thermophoresis through a boundary layer of air at the substrate[19] – to form a porous coating. More details of LFS method are given elsewhere.[17-19] Silicon dioxide and titanium dioxide were selected as coating materials since they are widely used in different coating applications such as painting,[21] cast-,[22] dip-,[23] spray-,[18] and vapor-phase[4] deposition. Titanium dioxide is well-known for its photocatalytic activity. This property can be utilized in self-cleaning coatings[24] and to decompose atmospheric pollutants such as nitrogen oxides (NO_x).[21]

We first investigate potential of a pure silicon dioxide coating (Si/Ti ratio = 100/0 wt% in the precursor) to form the overhang morphology. From now on, we call this "Si 100 wt% coating". The coating was synthesized on a smooth glass substrate by injecting TEOS diluted in isopropanol into the upwards pointing LFS flame, through which the sample was moved at a velocity of 0.8 m/s at the distance of 6 cm from the burner face. Scanning electron

microscopy shows that the resulting coating is ~100 nm thick and is composed of highly sintered, round sub-micrometer scale clusters evenly distributed on the surface (Figure 1a, g). After fluorination the surface shows moderate liquid repellency with apparent static contact angles of 138° for water (surface tension γ = 72.8 mN/m), 118° for ethylene glycol (γ = 47.3 mN/m, 99.8% pure, Sigma-Aldrich), and 83° for *n*-hexadecane (γ = 27.5 mN/m, 99% pure, Sigma-Aldrich).

To enhance liquid repellency, we use two approaches (Figure 1). Firstly, we substitute part of the silicon dioxide by titanium dioxide in the coating by adding TTIP to the precursor solution (Figure 1, leftmost column). Secondly, we increase the thickness of the coating by applying 5 LFS coating cycles prior to fluorination (Figure 1, middle column). To gain insight on the individual agglomerate morphology, we collected particles from LFS on transmission electron microscopy grids (Figure 1, rightmost column).

Already 1 wt% addition of titanium atoms with respect to silicon atoms in the precursor (Si/Ti ratio = 99/1 wt%) drastically changes the morphology of the coating. We call this "Si 99 wt% coating", Figure 1c, h. An energy dispersive x-ray spectroscopy (EDS/EDX) analysis indicates that the Si/Ti ratio within the coating is 96.2/3.8 wt% (Supporting Information, Figure S1, Table S1). The changes become more prominent when the titanium content was increased up to 99 wt% (Si/Ti ratio = 1/99 wt%). We call this "Si 1 wt% coating", Figure 1e, i, j. Silicon dioxide is no longer aggregated in highly sintered, dense clusters. Instead, the coating shows increasing amount of porous, nanosized particle aggregates with overhang structures. EDS analysis shows that the Si/Ti ratio within the coating is 2.1/97.9 wt%. Titanium dioxide has mainly anatase crystal structure with small amount, 10–15%, of rutile independently on the Si/Ti ratio. Silicon dioxide remains amorphous.[18] We speculate that these morphological changes are caused by an early nucleation of titanium dioxide in the

cooling flame while silicon dioxide remains still in vapor phase.[18, 19] Titanium dioxide particles thus act as nucleation sites for silicon dioxide and facilitate formation of the porous particle aggregates within the coating. Silicon dioxide, which sinters at lower temperature than titanium dioxide, acts as a "binding agent" within the coating and thus enhances its mechanical stability (see discussion with drop impact experiments).

Then we increase the coating thickness by moving the samples through the flame spray 5 sequential times at intervals of ~2 s. The growth mechanism of the coating through the boundary layer of air at the surface – driven by thermophoresis and diffusion – induces accumulative growth of large particle aggregates at the surface (Figure S2). As a consequence, the height of the surface protrusions and hierarchical roughness of the coating increase (Figure 1b, d, f, k; Figure S3; Figure S4). The final height of the surface textures depends on the coating composition. With highly sintered, dense Si 100 wt% coating the highest protrusions reach ~700 nm after 5 coating cycles (Figure S3). With Si 1 wt% coating the highest peaks of the surface texture are ~700 nm already after the first coating cycle (Figure 1j) and reach a height of at least 7 µm after 5 cycles (Figure 1k and Figure S4).

After a single LFS coating cycle, referred to as "thin coating", the best liquid repellency is given by Si 1 wt% coating. Water drops deposited on the surface adapt a spherical shape with static contact angle >160°. 10 µL sized drops roll off the surface as soon as the substrate is inclined by less than ~3°. With ethylene glycol and *n*-hexadecane, the static contact angles approach 150° but the drops pin to the surface, i.e. roll-off angles are typically >10° (**Table 1**).

A coating with superamphiphobic properties was achieved by coupling the two approaches, i.e. by reducing the amount of Si/Ti ratio in the precursor from 100/0 wt% to 1/99 wt% and by

increasing the number of coating cycles from 1 to 5, referred to as "thick coating". In this way we obtained a roll-off angle below 1° for 10 µL *n*-hexadecane drops. Advancing and receding contact angles were 165° with non-measurable contact angle hysteresis when the drop volume was increased and decreased between 15 and 25 µL at the rate of 1 µL/s using a standard contact angle goniometer (Figure S5, Video S1).

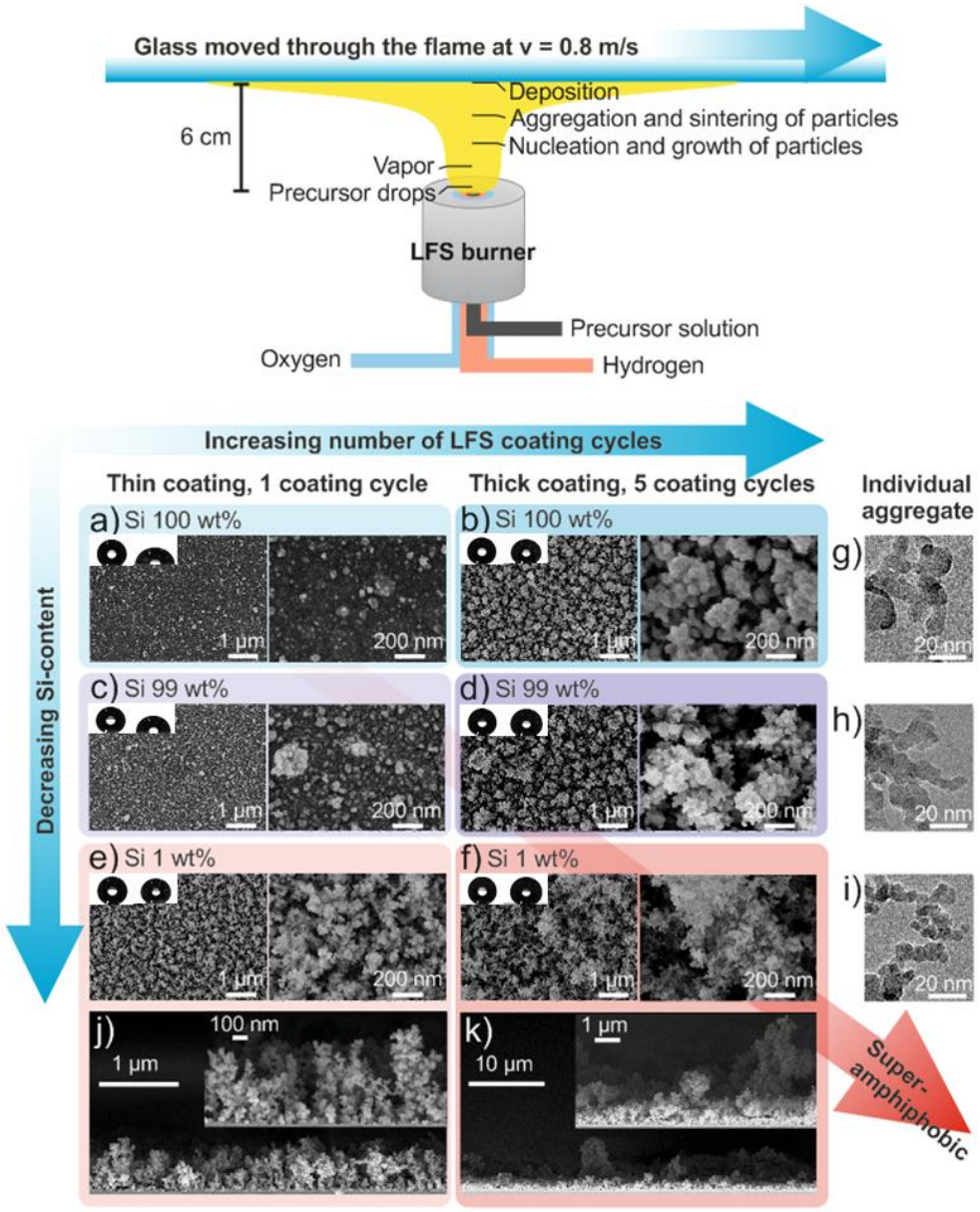

Figure 1. Synthesis and morphology of nanotextured liquid-repellent coatings by LFS. Top: schematic illustration of the coating procedure (not to scale). Bottom: Top-view scanning electron microscopy (SEM) images of the coatings with different silicon dioxide content and thickness after chemical vapor deposition (CVD) of the fluorosilane. a, b) Si 100 wt%; c, d) Si

99 wt%; and e, f) Si 1 wt% coating. Insets: the shape of 5 µL water (left) and *n*-hexadecane (right) drops resting on the respective surfaces. Transmission electron microscopy (TEM) images show different degree of sintering and overhang morphology of the particle aggregates: g) Si 100 wt%, h) Si 99 wt%, and i) Si 1 wt% coating. Side-view SEM images of j) Si 1 wt% thin coating (coated 1 time) and k) Si 1 wt% thick coating (coated 5 times).

Table 1. Wettability of the liquid-repellent coatings. Apparent static contact angles (CA) and roll-off angles (RA) of 10 µL drops of water, ethylene glycol, and *n*-hexadecane on coatings with different silicon dioxide content and thickness after chemical vapor deposition of the fluorosilane. "Thin" refers to a single LFS coating cycle. "Thick" refers to 5 subsequent LFS coating cycles. The standard deviations are given by individual contact angle goniometer measurements. Note that contact angles larger than ~155° cannot reliably be measured using the goniometer technique and thus the real error is larger.

Coating	Water CA/RA (°)	Ethylene glycol CA/RA (°)	n-hexadecane CA/RA (°)
Si 100 wt%, thin	138±3 / -	118±1 / -	83±1 / -
Si 100 wt%, thick	168±1 / <1	154±3 / 50±3	146±1 / -
Si 99 wt%, thin	157±4 / 13±10	126±5 / -	91±4 / -
Si 99 wt%, thick	168±1 / <1	160±5 / 6±1	153±2 / -
Si 1 wt%, thin	163±2 / 3±1	154±2 / 12±1	151±2 / 29±7
Si 1 wt%, thick	167±1 / <1	164±1 / <1	157±4 / 1±1

The superamphiphobic coating developed here shows extremely low interaction with water and even with *n*-hexadecane. To our knowledge, the lowest roll-off angles reported for *n*-hexadecane on superamphiphobic surfaces are 2–5° depending on the surface and the drop size.[2-5, 7, 9, 10, 16] Here, 10 µL drops of *n*-hexadecane typically rolled off the surface as soon as the goniometer needle tip was detached although the substrate was adjusted in horizontal plane without any apparent inclination angle (Video S2).

Our coating consists of random, overhang nanostructures where the diameter of spherical primary particles is ~10–20 nm. We investigated the effect of texture size on water repellency by growing an additional 20 nm thick silicon dioxide layer on the surface using a gas-phase Stöber-like reaction.[4] After growing the silicon dioxide layer (Figure S6) and modifying the surface with the fluorosilane, the anti-wetting performance declined. For all coating compositions (Si 100 wt%, Si 99 wt%, and Si 1 wt%) the water contact angle decreased and the roll-off angle increased due to the increased solid–liquid contact area and smoothed out overhangs as compared to the pristine coatings (Table S2). This underlines the role of nanosized texture in reducing the solid–liquid interactions on the coating. Coupling this nanosized texture with pronounced hierarchical surface roughness supports the air cushion below the liquids and leads to extremely small overall contact area between the coating and the liquids.

We expect that the extreme liquid repellency of the thick Si 1 wt% layer is caused by the hierarchical surface roughness in addition to the overhanging morphology on the 10 nm scale. A simple estimation on a surface consisting of spherical, randomly aggregated particles shows that this combination ensures low penetration depth and wetted contact area of both polar and non-polar liquids on the solid substrate, **Figure 2**. Knowing the mean radius of the particles r and the Young contact angle θ on the solid, fluorinated silicon oxide, the penetration depth δ around a single particle on the surface in thermodynamic equilibrium at zero external pressure can be estimated (Figure 2a, Supporting discussion) to be $\delta \approx 0.58r$ for water (θ = 115°) and $\delta \approx 1.29r$ for *n*-hexadecane (θ = 73°). Here, we assumed that the particle is fixed at the bottom. Taking into account the random packing in the porous structure, the number of wetted particles underneath the first layer of particles will increase before reaching θ (Figure 2b). This increase in the wetted contact area is larger for non-polar liquids than for polar, high-

surface tension liquids. That is, overhangs can support the air cushion below low-surface-tension liquids, however, the liquid still wets large surface area and therefore pins to the solid (Supporting discussion). To reduce the overall wetted area of the solid and thus adhesion of drops, hierarchical roughness needs to be introduced (Figure 2c). Indeed, several surfaces with inherent hierarchical roughness such as paper,[9] wood,[16] and fabrics[7] serve as ideal substrates for randomly structured superamphiphobic coatings where both polar and non-polar liquid drops can bead up and easily roll off the surface.

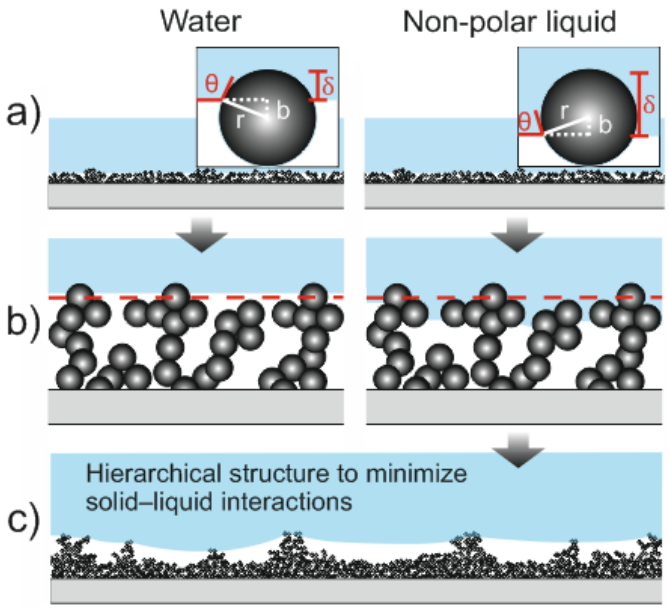

Figure 2. Schematic illustration of wetting of a model surface by water and a non-polar liquid. The surface consists of spherical particles. Penetration depth δ of the liquid around a single particle with radius r depends on the intrinsic wettability of the material, characterized by the Young contact angle θ. a) Water (large θ) wets small fraction of individual particles within the first particle layer, indicated by the dashed line in b). A non-polar liquid (small θ) wets large fraction of individual particles and b) invades from one particle to the other into the texture of the solid until θ is reached at the overhangs. c) Hierarchical roughness of the surface has critically important role in reducing the overall solid–liquid contact area and pinning of low-surface-tension liquids on randomly structured superamphiphobic surfaces.

To achieve superamphiphobicity, a nanoscopic overhanging structure needs to be combined with roughness on the >1 µm length scale; in the following we call this a *hierarchical structure*. Such hierarchical structures need a certain minimum coating thickness. Below this minimum thickness, it might not be possible to create a superamphiphobic surface. The overall solid–liquid contact area would become too large. This condition poses a lower limit to the thickness of a superamphiphobic coating on a smooth substrate such as plain glass. Here the coating was not superamphiphobic after one coating cycle when its thickness was ~700 nm (Figure 1j). However, after 5 coating cycles the coating became superamphiphobic (Figure 1k and Figure S4). It is reasonable to assume that with most of the randomly structured superamphiphobic surfaces, the hierarchical surface structure increases with increasing coating thickness. For example, the candle soot templated coating remains superamphiphobic only when the coating is thicker than ~2 µm.[4, 25]

We verify optical transparency of our coatings by ultraviolet-visible light transmittance spectroscopy. All thin coatings (coated 1 time) transmit more than 98% as compared to the transmittance through the pristine glass substrate (for wavelengths higher than 500 nm, Figure S7). Thick coatings (coated 5 times) transmit 97% of the light for Si 100 wt% coating and 79% for Si 1 wt% coating (**Figure 3a**). High transmittance of light at the visible light spectrum results in good optical transparency (Figure 3b) of the super liquid-repellent coatings (Figure 3c).

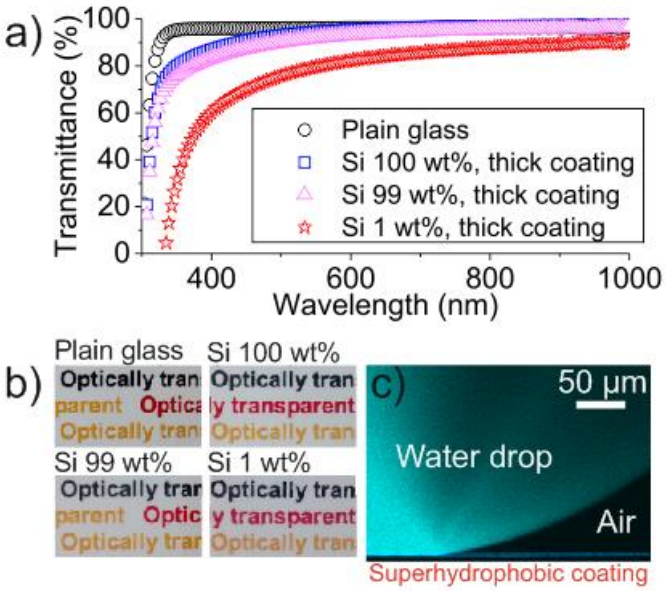

Figure 3. Optical transparency of the liquid repellent coatings. a) Ultraviolet-visible light transmittance spectra of glass before and after the coating. b) Photographs of the thick coatings (coated 5 times) on glass. Printed letters on paper are visible below the liquid repellent coatings. c) Laser scanning confocal microscopy (LSCM) image of a 0.5 µL water drop resting on a ~700-nm-thick superhydrophobic coating on a glass substrate (Si 100 wt%, thick coating). The drop was fluorescently labeled with Atto 488 hydrophilic dye at the concentration of 1 µg/mL.

In addition to liquid repellency and optical transparency, the impalement resistance of the coating decides about potential applications. How stable is the Cassie-Baxter state before the whole surface texture is wetted by the liquid and the system goes to the so-called Wenzel state?[26] We investigate the impalement resistance of our superamphiphobic coating by letting water drops impact the surface from different heights. Water drops of 15 µL volume (radius R = 1.5 mm) were released from heights of 1–200 cm leading to impact velocities v between 0.4 m/s and 5.4 m/s. This approaches the terminal velocity of falling medium-sized rain drops (R <1 mm).[27] Such an impact velocity and drop radius corresponds to Weber numbers up to

$We = \rho v^2 R/\gamma \approx 600$. Here, ρ is the density of water = 1 g/cm^3. The drops always rebounded from the surface and no impalement was observed.

To prevent full or partial penetration of the impinging drops,[11] the capillary pressure P_C generated within the textures should be higher than the maximal effective hammer pressure P_E, which is the upper limit for the pressure the surface can experience during the impact.[28] For drops impacting on horizontal flat surface one can estimate the maximal hammer pressure:[28]

$$P_E \approx 0.2\rho C v. \quad (1)$$

Here, C is the sound velocity (for water C = 1497 m/s). For an impact velocity v = 5.4 m/s and water the hammer pressure can be estimated to be 1.6 MPa. The maximal capillary pressure developed within the particle-like surface texture to prevent the impalement can be estimated from[29]

$$P_C \approx \frac{2\gamma r}{d^2} sin^2 \frac{\theta_{adv}}{2}. \quad (2)$$

Here, *d* is the mean distance between protrusions, r is the radius of the constituting particles and θ_{adv} = 119° is the advancing contact angle of water on a smooth fluorosilane coated silicon oxide. When the hammer pressure P_E exceeds P_C one expects the Cassie-Baxter state to collapse. With roughly r = 5–10 nm and setting $P_E = P_C$ we get a required maximal spacing of protrusions = 18–26 nm. On our coating, the smallest pores between the particles and their aggregates can fulfill this criterion (Figure 1f, i). It is expected that the liquid will penetrate in between the largest protrusions on the surface. These protrusions dampen the

impact and relief the pressure experienced by the surface in between them. For comparison, on a rectangular array of the fluorosilane modified SU8 micropillars with solid area fraction of 0.06 (5 µm side wall, 10 µm height, 15 µm spacing, fabricated by photolithography[30]) impalement of impacting 15 µL water drops occurred already at the hammer pressure of ~240 kPa (release height = 3 cm, impact v = 0.8 m/s, We = 12).

The superamphiphobic coating also repels impalement of impacting *n*-hexadecane drops (R = 1 mm, ρ = 0.773 g/cm^3, **Figure 4**). At 1 cm release height the 5 µL drop bounced 4 times before settling down at the surface (Video S3, v = 0.4 m/s, We = 5.4). At 10 cm release height the drop bounced 6 times before settling down (Video S4, v = 1.4 m/s, We = 55). The *n*-hexadecane drops even rebound when released from a height of 50 cm. The corresponding impact velocity for the drop was 3 m/s (We = 250). Calculating the pressure experienced by the surface during impact of the *n*-hexadecane drop with equation 1 and a speed of sound in *n*-hexadecane = 1339 m/s[31] we get P_E = 650 kPa. Assuming that this pressure is balanced by the capillary pressure (equation 2) a protrusion spacing of maximal d = 13–18 nm is allowed when θ_{adv} = 77° is the advancing contact angle of *n*-hexadecane on a smooth fluorosilane coated silicon oxide. This is in the same order of magnitude that we got for the maximal spacing with water.

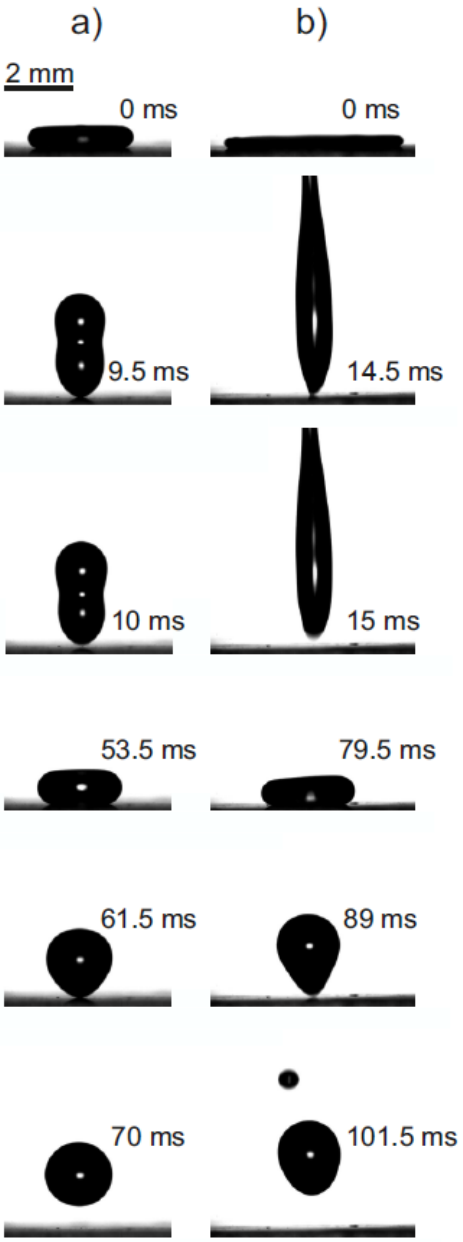

Figure 4. 5 µL *n*-hexadecane drops (R = 1 mm) impinging the superamphiphobic surface at different velocities. The snapshot images of a high-speed camera (2000 fps) show the maximum spreading and take off of the drops within the first and the second rebound at the surface at a) impingement velocity v = 0.4 m/s (release height = 1 cm, We = 5.4) and b) v = 1.4 m/s (release height = 10 cm, We = 55). At the higher impingement velocity v = 1.4 m/s the drop generated a satellite drop within the impact, which is merging with the main drop after the second rebound.

The mechanical stability of the superamphiphobic coating was tested by letting 15 µL water drops impact on the surface from the release height of 200 cm at v = 5.4 m/s. The sample was tilted by 10° to ensure rapid removal of the impinging drops. The coating could withstand at least 20,000 drop impacts (90 impacts/min) by completely allowing the impinging drops to bounce off the surface. After the experiment, roll-off angle of 10 µL water drops at the impacted area was 13°. The nanotexture was partially damaged and hexadecane drops started to pin to the impacted surface (Figure S8). With increasing silicon dioxide content the mechanical stability of the coating increased against impacting drops. After 20,000 drop impacts on both the Si 100 wt% and Si 99 wt% coating the roll-off angle of 10 µL water drops remained at 3–5°. That is, the surfaces remained superhydrophobic after the exposure to the impacting drops.

Robustness of the superamphiphobic coating (Si 1 wt%, coated 5 times) was further tested by exposing the surface to different stresses. Adhesion of the coating to the glass substrate was evaluated by exposing the surface to steam and condensing water. Therefore, water was heated in a beaker on a hot plate at 150°C and the sample was placed face down 5 cm above the water surface for 1 h. A coating adhered only by van der Waals forces would delaminate. Here, roll-off angle for 10 µL water drops remained <1°, which indicates good adhesion of the coating to the substrate. The strong capillary forces of the condensing water, however, partially destroyed the coating and *n*-hexadecane drops started to pin.

Additionally, adhesion of the coating was tested by adhering and peeling off an adhesive tape (Scotch Magic), applied with the pressure = 2.5 kN/m^2 for 60 s. After the tape test, the coating maintained low roll-off angle for both water and *n*-hexadecane, <1° and 6±2°, respectively.

Abrasion by impacting sand particles partially destroyed the coating. After impacting the surface with 100–200 μm diameter sand grains from the height of 2 cm for 10 s (5 g of sand; sample was adjusted at an angle of 45°), *n*-hexadecane drops pinned to the surface. However, water drops showed high static contact angle = 155° and roll-off angle = 25° after the abrasion, which indicates that the failure of the coating was cohesive. More robust Si 100 wt% coating remained superhydrophobic even after the sand abrasion proven by the low roll-off angle = 2° for 10 μL water drops.

Temperature-stability of the superamphiphobic Si 1 wt% coating was investigated between −200°C and +500°C. Delamination of the coating was not observed even after freezing the sample in liquid nitrogen for ~30 s (Figure S9). Roll-off angles for water and *n*-hexadecane remained <1° and 10±5°, respectively. Heating the sample in an oven at 500°C for 3 h degraded the fluorosilane layer. After re-applying the fluorosilane, the coating recovered its high static contact angle >160° and low roll-off angle <1° for both water and *n*-hexadecane.

Photosensitivity of the superamphiphobic coating was investigated by illuminating the surface with UV-A light (2.3 ± 0.3 mW/cm^2) up to 4 h. Titanium dioxide is photocatalytically active. Already after 40 min of illumination, 10 μL drops of *n*-hexadecane pinned to the surface (Table S3) because of photodegradation of the fluorosilane coating on top. To prevent this, before the fluorination we encapsulated the coating with a ~3-nm-thick silicon dioxide shell by applying the gas-phase Stöber-like reaction for 4 hours. Such a thin passivation layer did not hinder the superamphiphobic properties of the coating. Moreover, the coating remained superamphiphobic even after the UV-A illumination of 4 h: roll-off angles for 10 μL water and *n*-hexadecane drops were <1° and 4°, respectively.

Robustness of the air cushion on the superamphiphobic coating under prolonged contact with *n*-hexadecane was investigated by letting the 10 µL drops to rest on the surface for 30 min. The static contact angle remained unchanged within the experimental error (Figure S10). After the period of 30 min, roll-off angle for the *n*-hexadecane drops was 10±2°, proving the stability of the air cushion.

In summary, we introduce an up-scalable method to fabricate optically transparent superamphiphobic surfaces with low drop adhesion and high impalement resistance against both high- and low-surface-tension liquids. With LFS and by mixing Si and Ti precursors, surfaces can be fabricated with high apparent contact angles and low roll-off angles below ~1° even for *n*-hexadecane. To achieve an ultra-low drop adhesion for non-polar liquids, the superamphiphobic surface needs to fulfill the following criteria: (1) low-surface-energy chemistry, (2) nanoscale, overhang surface structures, (3) hierarchical roughness, and (4) sub-micron scale pore size to increase the critical impalement pressure. We show that increased Ti content in the coating and increased number of coating cycles increase porosity, thickness, and hierarchical structure of the coating. This improves the superamphiphobic properties. On the other hand, optical transparency of the coating decreases and better mechanical stability is achieved with high Si content. Si/Ti ratio needs to be optimized depending on the requirements for the coating.

Experimental Section

Surface modification: Prior to chemical vapor deposition (CVD) with the fluorosilane the samples were activated by oxygen plasma (Femto low-pressure plasma system, Diener electronic, Germany) at 300 W for 10 min. The samples were placed in a desiccator together with 100 µL of the fluorosilane and the pressure was reduced to ~200 mbar for 2h. After the CVD, the samples were placed in a vacuum oven at 60°C for 2h to remove unreacted silane.

For the gas-phase Stöber-like reaction, selected samples were placed in a desiccator together with ammonia (3 mL) and TEOS (3 mL) at atmospheric pressure and room temperature for 24 h. This resulted in growth of an additional 20-nm-thick porous silicon dioxide shell around the particles.[4] After the silicon dioxide growth, the samples were sintered in an oven at 500°C for 3 h and subsequently fluorinated by the CVD process. To prevent photocatalytic degradation of the fluorosilane, the superamphiphobic surface was passivated by growing a ~3 nm thick silicon dioxide layer on the coating by applying the gas-phase Stöber-like reaction for 4 h. After this, the coating was fluorinated by CVD. The coating was not sintered in the oven.

Microscopy/Spectroscopy: For SEM imaging (LEO 1530 Gemini, Zeiss), the samples were sputter-coated with a nm-thick Pt layer to reduce the surface charging. The used sputtering time would yield a layer thickness of ~7 nm on a smooth substrate. TEM imaging was performed with JEOL JEM-2010 instrument. The samples were collected on lacey carbon film on copper grid (Agar) directly from LFS at the distance of 6 cm from the burner face by moving the grid through the flame at the velocity of 0.8 m/s. Chemical composition of the coatings was investigated using Hitachi SU8000 SEM equipped with EDS/EDX. For the analysis the porous oxide coatings (coated 5 times) were scraped from the glass substrate onto a conductive carbon tape to exclude any Si signal originating from the substrate. At least 3 measurements at different positions were conducted. An inverted laser scanning confocal microscope (Leica TCS SP8 SMD, Leica Microsystems) with HC PL APO CS2 40x/1.10 water objective was used to capture a micrograph of a water drop resting on Si 100 wt% surface.

Wetting properties: Static contact angles with 5 µL drops and roll-off angles with 10 µL drops of water, ethylene glycol, and *n*-hexadecane were measured by DataPhysics OCA 35

goniometer (DataPhysics Instruments) using 3 to 5 individual measurements at different positions on each sample. Static contact angles larger than 155° cannot reliably be measured using the goniometer technique as for high contact angles real position of the base line is difficult to determine and even small variation greatly influences the measured values. Although the measured values may be too low, the trend should be correct. Advancing and receding contact angles were measured by increasing the drop volume from 0 to 25 µL and decreasing the volume back to ~0 µL at the rate of 1 µL/s. The dynamic contact angles were carefully analyzed using Fiji,[32] an open-source image processing software. Contact angle hysteresis was determined using drop volumes of 15–25 µL to prevent that the goniometer needle affected the results.[33] Impingement dynamics of 5 µL *n*-hexadecane drops were investigated using Photron Fastcam Mini UX100 high-speed camera (2000 fps).

Illumination and light transmittance: The samples were illuminated by UV-A light (intensity = 2.3 ± 0.3 mW/cm^2) from the distance of 8 cm (light source: LQ-400, Dr. Gröbel UV-Elektronik GmbH) up to 4 h to verify the passivation effect of the 3-nm-thick silicon dioxide shell on the photocatalytic activity of titanium dioxide. Intensity of the illumination was measured using an UV-radiometer RM-12 with UV-A sensor for spectral range of 315–400 nm (Dr. Gröbel UV-Elektronik GmbH). Ultraviolet-visible light (UV-Vis) spectrometer (Lambda 25, PerkinElmer) was used to investigate light transmittance of the coatings.

Supporting Information

Supporting Information is available from the Wiley Online Library or from the author.

Acknowledgements

This work was funded by the ERC advanced grant 340391 – SUPRO, the Collaborative Research Center 1194, and the European Union's Horizon 2020 research and innovation

program LubISS No 722497. H.T. acknowledges Tekes – the Finnish Funding Agency for Innovation (grant 40365/14), Walter Ahlström Foundation (Tutkijat maailmalle –program), and Alexander von Humboldt Foundation for financial support. Dr. Mari Honkanen and Prof. Jurkka Kuusipalo (Tampere University of Technology) are acknowledged for the TEM images and for providing the paper substrate. Mr. Gunnar Glasser is acknowledged for the EDS/EDX analysis. Ms. Olinka Ramirez and Dr. Jonathan Pham are acknowledged for technical support.

Received: ((will be filled in by the editorial staff))
Revised: ((will be filled in by the editorial staff))
Published online: ((will be filled in by the editorial staff))

References

[1] K. Tsujii, T. Yamamoto, T. Onda, S. Shibuichi, Angew. Chem. Int. Ed. Engl. 1997, 36, 1011.

[2] A. Tuteja, W. Choi, M. Ma, J. M. Mabry, S. A. Mazzella, G. C. Rutledge, G. H. McKinley, R. E. Cohen, Science 2007, 318, 1618.

[3] J. Zhang, S. Seeger, Angew. Chem. Int. Ed. Engl. 2011, 50, 6652.

[4] X. Deng, L. Mammen, H.-J. Butt, D. Vollmer, Science 2012, 335, 67.

[5] Z. Chu, S. Seeger, Chem. Soc. Rev. 2014, 43, 2784.

[6] F. Schellenberger, N. Encinas, D. Vollmer, H.-J. Butt, Phys. Rev. Lett. 2016, 116, 096101.

[7] A. K. Kota, G. Kwon, A. Tuteja, NPG Asia Mater. 2014, 6, e109.

[8] M. Paven, P. Papadopoulos, S. Schöttler, X. Deng, V. Mailänder, D. Vollmer, H. J. Butt, Nature Comm. 2013, 4, 2512.

[9] L. Jiang, Z. Tang, R. M. Clinton, V. Breedveld, D. W. Hess, ACS Appl. Mater. Interfaces 2017, 9, 9195.

[10] F. Geyer, C. Schönecker, H.-J. Butt, D. Vollmer, Adv. Mater. 2017, 29.

[11] D. Bartolo, F. Bouamrirene, É. Verneuil, A. Buguin, P. Silberzan, S. Moulinet, Europhys. Lett. 2006, 74, 299; M. Reyssat, A. Pépin, F. Marty, Y. Chen, D. Quéré, Europhys. Lett. 2006, 74, 306; Y. Liu, L. Moevius, X. Xu, T. Qian, J. M. Yeomans, Z. Wang, Nat. Phys. 2014, 10, 515.

[12] A. B. D. Cassie, S. Baxter, Trans. Faraday Soc. 1944, 40, 546.

[13] T. Liu, C.-J. Kim, Science 2014, 346, 1096.

[14] R. Dufour, P. Brunet, M. Harnois, R. Boukherroub, V. Thomy, V. Senez, Small 2012, 8, 1229; A. G. Marín, H. Gelderblom, A. Susarrey-Arce, A. van Houselt, L. Lefferts, J. G. Gardeniers, D. Lohse, J. H. Snoeijer, Proc. Natl. Acad. Sci. U.S.A. 2012, 109, 16455.

[15] H. Teisala, M. Tuominen, J. Kuusipalo, Adv. Mater. Interfaces 2014, 1, 1300026; Y. Si, Z. Guo, Nanoscale 2015, 7, 5922; W. S. Wong, G. Liu, N. Nasiri, C. Hao, Z. Wang, A. Tricoli, ACS Nano 2017, 11, 587; W. Cui, T. Wang, A. Yan, S. Wang, Appl. Surf. Sci. 2017, 400, 162; X. Zhu, Z. Zhang, G. Ren, X. Men, B. Ge, X. Zhou, J. Colloid Interface Sci. 2014, 421, 141.

[16] M. Tuominen, H. Teisala, J. Haapanen, J. M. Mäkelä, M. Honkanen, M. Vippola, S. Bardage, M. E. P. Wålinder, A. Swerin, Appl. Surf. Sci. 2016, 389, 135.

[17] H. Teisala, M. Tuominen, M. Aromaa, J. M. Mäkelä, M. Stepien, J. J. Saarinen, M. Toivakka, J. Kuusipalo, Surf. Coat. Technol. 2010, 205, 436.

[18] J. Haapanen, M. Aromaa, H. Teisala, M. Tuominen, M. Stepien, J. J. Saarinen, M. Heikkilä, M. Toivakka, J. Kuusipalo, J. M. Mäkelä, Mater. Chem. Phys. 2015, 149-150, 230.

[19] J. M. Mäkelä, M. Aromaa, H. Teisala, M. Tuominen, M. Stepien, J. J. Saarinen, M. Toivakka, J. Kuusipalo, Aerosol Sci. Technol. 2011, 45, 827.

[20] H. Teisala, M. Tuominen, M. Aromaa, M. Stepien, J. M. Makela, J. J. Saarinen, M. Toivakka, J. Kuusipalo, Langmuir 2012, 28, 3138.

[21] N. S. Allen, M. Edge, J. Verran, J. Stratton, J. Maltby, C. Bygott, Polym. Degrad. Stab. 2008, 93, 1632.

[22] R. A. Caruso, in *Topics in current chemistry: Colloid chemistry 1*, Vol. 226, Springer-Verlag Berlin, Germany 2003, 91.

[23] L. Xu, J. He, Langmuir 2012, 28, 7512.

[24] Y. Paz, Z. Luo, L. Rabenberg, A. Heller, J. Mater. Res. 2011, 10, 2842; S. Wooh, N. Encinas, D. Vollmer, H.-J. Butt, Adv. Mater. 2017, 29, 1604637.

[25] M. Paven, P. Papadopoulos, L. Mammen, X. Deng, H. Sachdev, D. Vollmer, H.-J. Butt, Pure Appl. Chem. 2014, 86, 87.

[26] R. N. Wenzel, Ind. Eng. Chem. 1936, 28, 988.

[27] J. O. Laws, Trans. Am. Geophys. Union 1941, 22, 709.

[28] T. Deng, K. K. Varanasi, M. Hsu, N. Bhate, C. Keimel, J. Stein, M. Blohm, Appl. Phys. Lett. 2009, 94, 133109; O. G. Engel, J. Res. Natl. Bur. Stand. 1955, 54, 281.

[29] M. Ye, X. Deng, J. Ally, P. Papadopoulos, F. Schellenberger, D. Vollmer, M. Kappl, H.-J. Butt, Phys. Rev. Lett. 2014, 112, 016101; H.-J. Butt, C. Semprebon, P. Papadopoulos, D. Vollmer, M. Brinkmann, M. Ciccotti, Soft Matter 2013, 9, 418.

[30] F. Schellenberger, J. Xie, N. Encinas, A. Hardy, M. Klapper, P. Papadopoulos, H.-J. Butt, D. Vollmer, Soft Matter 2015, 11, 7617.

[31] S. Outcalt, A. Laesecke, T. J. Fortin, J. Chem. Thermodyn. 2010, 42, 700.

[32] J. Schindelin, I. Arganda-Carreras, E. Frise, V. Kaynig, M. Longair, T. Pietzsch, S. Preibisch, C. Rueden, S. Saalfeld, B. Schmid, J. Y. Tinevez, D. J. White, V. Hartenstein, K. Eliceiri, P. Tomancak, A. Cardona, Nat. Methods 2012, 9, 676.

[33] J. T. Korhonen, T. Huhtamäki, O. Ikkala, R. H. A. Ras, Langmuir 2013, 29, 3858.

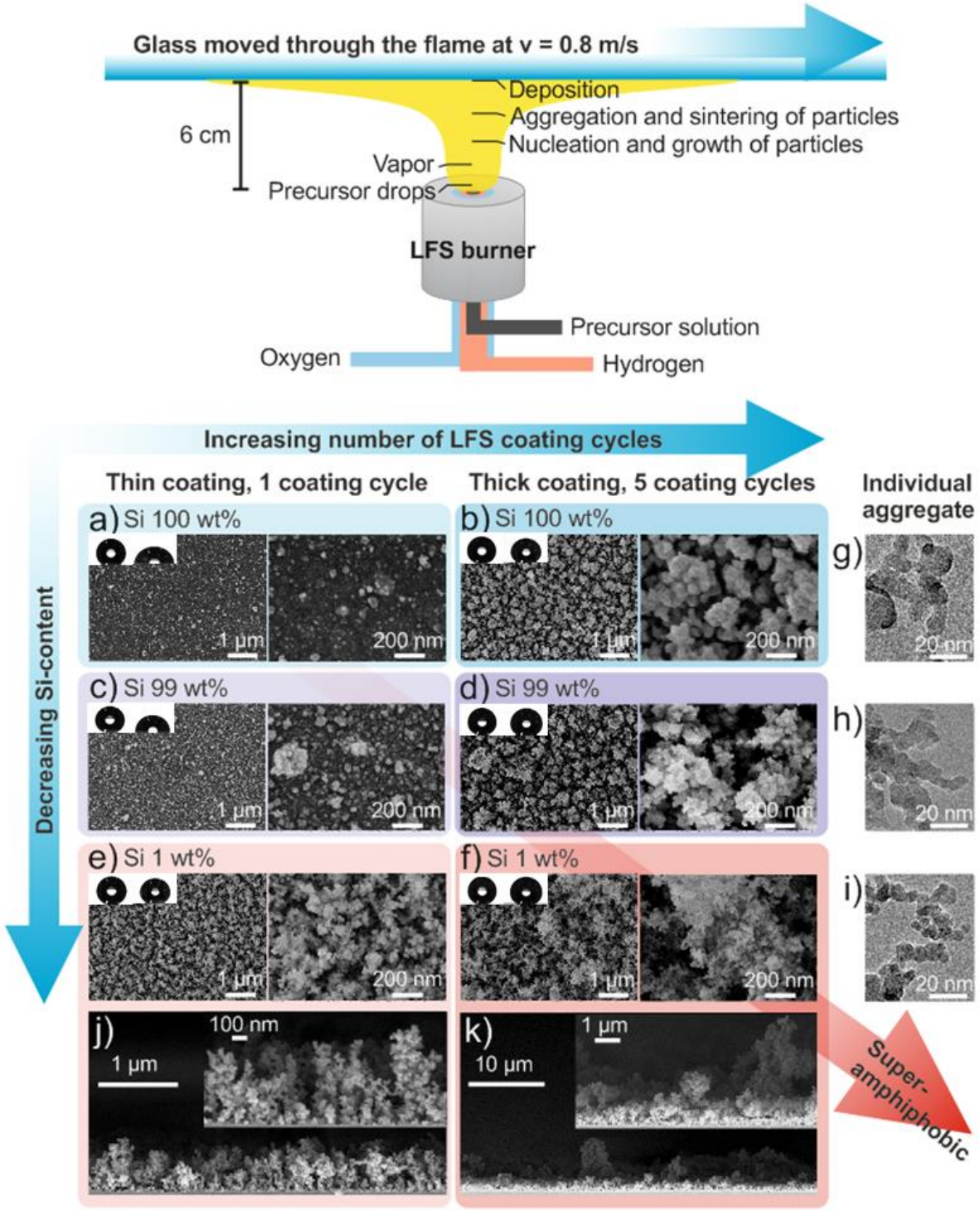

Figure 1. Synthesis and morphology of nanotextured liquid-repellent coatings by LFS. Top: schematic illustration of the coating procedure (not to scale). Bottom: Top-view scanning electron microscopy (SEM) images of the coatings with different silicon dioxide content and thickness after chemical vapor deposition (CVD) of the fluorosilane. a, b) Si 100 wt%; c, d) Si 99 wt%; and e, f) Si 1 wt% coating. Insets: the shape of 5 µL water (left) and *n*-hexadecane

(right) drops resting on the respective surfaces. Transmission electron microscopy (TEM) images show different degree of sintering and overhang morphology of the particle aggregates: g) Si 100 wt%, h) Si 99 wt%, and i) Si 1 wt% coating. Side-view SEM images of j) Si 1 wt% thin coating (coated 1 time) and k) Si 1 wt% thick coating (coated 5 times).

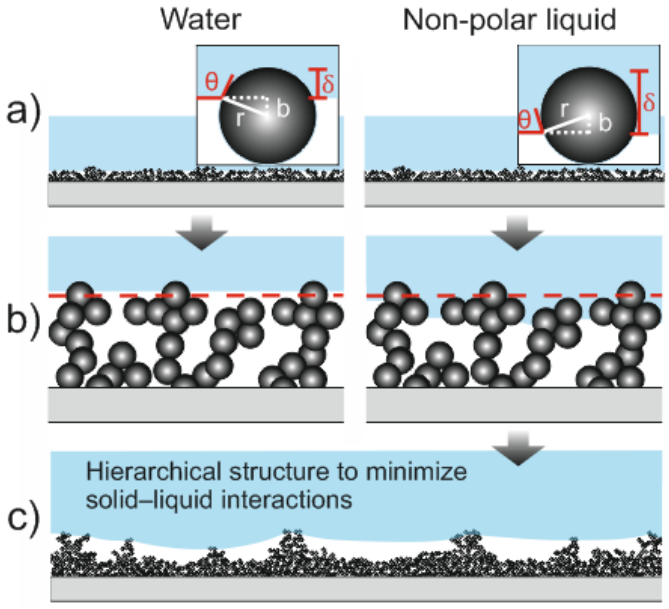

Figure 2. Schematic illustration of wetting of a model surface by water and a non-polar liquid. The surface consists of spherical particles. Penetration depth δ of the liquid around a single particle with radius r depends on the intrinsic wettability of the material, characterized by the Young contact angle θ. a) Water (large θ) wets small fraction of individual particles within the first particle layer, indicated by the dashed line in b). A non-polar liquid (small θ) wets large fraction of individual particles and b) invades from one particle to the other into the texture of the solid until θ is reached at the overhangs. c) Hierarchical roughness of the surface has critically important role in reducing the overall solid–liquid contact area and pinning of low-surface-tension liquids on randomly structured superamphiphobic surfaces.

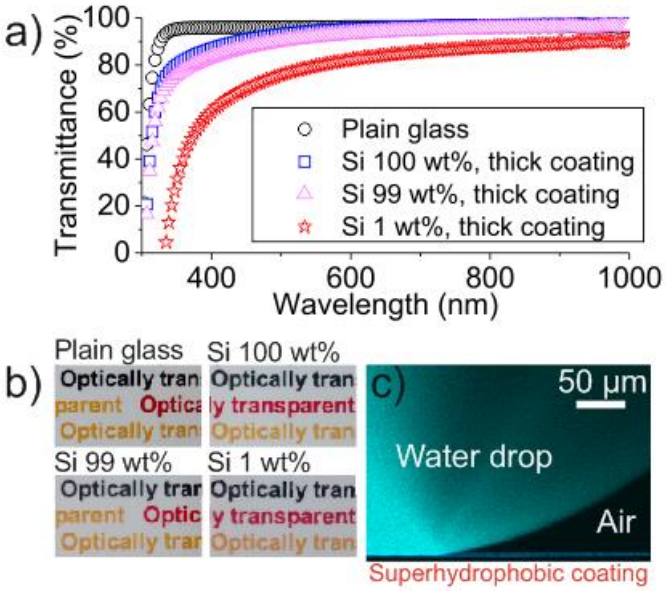

Figure 3. Optical transparency of the liquid repellent coatings. a) Ultraviolet-visible light transmittance spectra of glass before and after the coating. b) Photographs of the thick coatings (coated 5 times) on glass. Printed letters on paper are visible below the liquid repellent coatings. c) Laser scanning confocal microscopy (LSCM) image of a 0.5 µL water drop resting on a ~700-nm-thick superhydrophobic coating on a glass substrate (Si 100 wt%, thick coating). The drop was fluorescently labeled with Atto 488 hydrophilic dye at the concentration of 1 µg/mL.

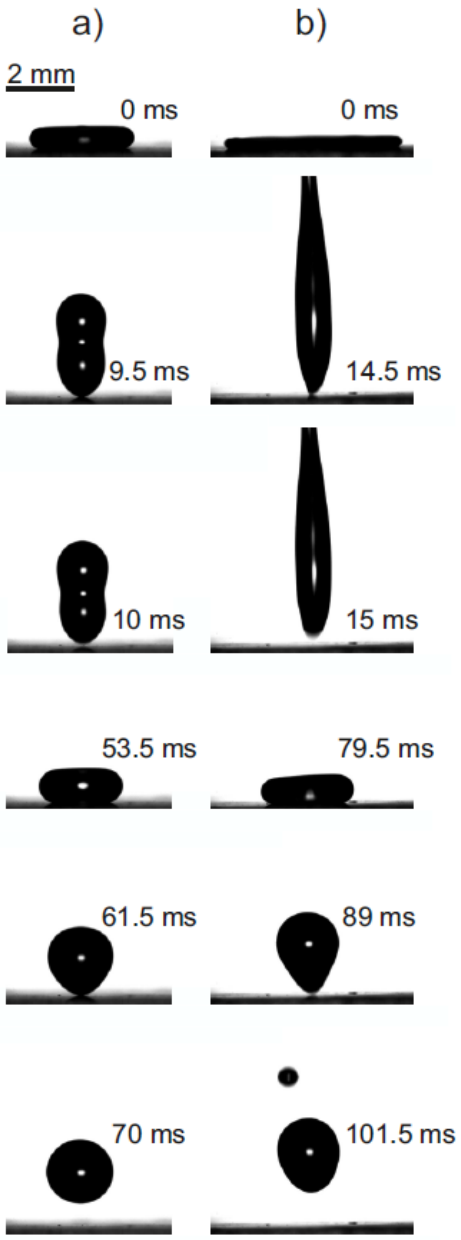

Figure 4. 5 µL *n*-hexadecane drops (R = 1 mm) impinging the superamphiphobic surface at different velocities. The snapshot images of a high-speed camera (2000 fps) show the maximum spreading and take off of the drops within the first and the second rebound at the surface at a) impingement velocity v = 0.4 m/s (release height = 1 cm, We = 5.4) and b) v = 1.4 m/s (release height = 10 cm, We = 55). At the higher impingement velocity v = 1.4 m/s the drop generated a satellite drop within the impact, which is merging with the main drop after the second rebound.

Table 1. Wettability of the liquid-repellent coatings. Apparent static contact angles (CA) and roll-off angles (RA) of 10 µL drops of water, ethylene glycol, and *n*-hexadecane on coatings with different silicon dioxide content and thickness after chemical vapor deposition of the fluorosilane. "Thin" refers to a single LFS coating cycle. "Thick" refers to 5 subsequent LFS coating cycles. The standard deviations are given by individual contact angle goniometer measurements. Note that contact angles larger than ~155° cannot reliably be measured using the goniometer technique and thus the real error is larger.

Coating	Water CA/RA (°)	Ethylene glycol CA/RA (°)	n-hexadecane CA/RA (°)
Si 100 wt%, thin	138±3 / -	118±1 / -	83±1 / -
Si 100 wt%, thick	168±1 / <1	154±3 / 50±3	146±1 / -
Si 99 wt%, thin	157±4 / 13±10	126±5 / -	91±4 / -
Si 99 wt%, thick	168±1 / <1	160±5 / 6±1	153±2 / -
Si 1 wt%, thin	163±2 / 3±1	154±2 / 12±1	151±2 / 29±7
Si 1 wt%, thick	167±1 / <1	164±1 / <1	157±4 / 1±1

The table of contents entry

Superamphiphobic surfaces can repel both water and oils. Impalement pressure and mechanical stability are still challenges. Fabrication is typically slow or expensive. Using liquid flame spraying we demonstrate an up-scalable method for fabricating SiO_2/TiO_2 nanostructured coatings at a velocity of 0.8 m/s. After fluorosilanization, the coating shows extremely low roll-off angles even towards *n*-hexadecane, high impalement pressure, and good transparency.

Keywords: wetting, superhydrophobic, superoleophobic, omniphobic, spray coating

H. Teisala*, F. Geyer, J. Haapanen, P. Juuti, J.M. Mäkelä, D. Vollmer, H.-J. Butt*

Ultra-fast processing of hierarchical nanotexture for a transparent superamphiphobic coating with extremely low roll-off angle and high impalement pressure